Exploring the third dimension in quantum confinement of surface electrons

Lu Lyu, Tobias Eul, Wei Yao, Jin Xiao, Mostafa Ashoush, Zakaria M. Abd El-Fattah, Ignacio Piquero-Zulaica, Johannes V. Barth, Martin Aeschlimann, Benjamin Stadtmüller

Angaben zur Veröffentlichung / Publication details:

Lyu, Lu, Tobias Eul, Wei Yao, Jin Xiao, Mostafa Ashoush, Zakaria M. Abd El-Fattah, Ignacio Piquero-Zulaica, Johannes V. Barth, Martin Aeschlimann, and Benjamin Stadtmüller. 2026. "Exploring the third dimension in quantum confinement of surface electrons." *Science Advances* 12 (24): eaed3926. https://doi.org/10.1126/sciadv.aed3926.

CONDENSED MATTER PHYSICS

Exploring the third dimension in quantum confinement of surface electrons

Lu Lyu[1,2]*, Tobias Eul[1,2], Wei Yao[1], Jin Xiao[3], Mostafa Ashoush[4], Zakaria M. Abd El-Fattah[4,5], Ignacio Piquero-Zulaica[6,7], Johannes V. Barth[8], Martin Aeschlimann[1], Benjamin Stadtmüller[1,2]*

Quantum confinement of surface electrons in two-dimensional metal-organic networks offers a powerful route to engineer electronic states for quantum and spintronic technologies. Here, we demonstrate the pivotal role of vertical variations in the surface potential on the quantum confinement of surface electrons. We investigate the confinement of both Shockley surface state and image-potential state electrons with their distinct vertical electron density distributions in a Cu-T4PT network on Cu(111). We find a substantial renormalization of the band mass of the image state, whereas the Shockley state remains almost unchanged. This notable divergence arises from the distinct three-dimensional potential landscape of the Cu-T4PT network, with a strong repulsive potential at the vertical position of the molecular backbone and leaky channels beneath the Cu coordination spheres. Our findings demonstrate the essential role of vertical potential engineering in designing quantum-confined states, thereby advancing control over electronic properties and quantum phenomena at the nanoscale.

INTRODUCTION

Quantum confinement of electrons and other (quasi-) particles within artificial nanostructures on surfaces provides an intriguing opportunity to explore the superior functionalities of quantum mechanics laws in condensed matter systems. Along these lines, the exploitation of phenomena such as quantum states coherence and coherent transport is of paramount importance for the realization of quantum technologies such as quantum computing on the solid-state platform. A key milestone in accessing the quantum world on surfaces was initially the atomic manipulation schemes involving scanning tunneling microscopy (STM) tips, which enabled the creation of tailor-made artificial nanostructures such as quantum corrals (*1*), one-dimensional (1D) gratings (*2*), and even 2D lattices (*3*). Pioneering studies thereby demonstrated quantized electronic states in functional quantum corrals (*4*) and notable quantum mirages (*5*). However, atomic manipulation protocols reached their practical limitations when applied to larger, periodic nanoarchitectures composed of hundreds or even thousands of atoms or molecules. In contrast, surface self-assembly, for instance, of organic molecules and metal atoms adsorbed into 2D metal-organic porous networks (2D-MOPNs) has emerged as an efficient alternative for constructing highly ordered and coupled quantum dot arrays (*6*). The unique advantage of such 2D-MOPNs lies in their chemical tunability, which allows precise control over the size, shape, and periodicity of nanoporous architectures through molecular design and intercomponent interactions (*7*). This tunable platform has enabled the observation of quantum confined states within network pores and the realization of engineered 2D band structures arising from the controlled coupling between neighboring quantum dots on metal surfaces (*8*, *9*).

Despite considerable progress, fundamental challenges persist in fully harnessing quantum-confined states within functional nanostructures for applications in information and quantum technologies. A central simplification in understanding quantum confinement of surface electrons, one that we seek to revisit, is the widespread assumption of a purely 2D surface potential landscape (*10*), as schematically illustrated in Fig. 1A. In the conventional models, the potential confining the surface state (SS) ψ_0 (green) is treated as a uniform barrier V_0 at the molecular backbone. The coordinating metal centers contribute to weakly repulsive, or even attractive, local potential channels that introduce in-plane variations in electron confinement across the metal-organic network. These spatial variations in the plane of the metal-molecule network structure have been successfully modeled by semiempirical simulations using electron plane wave expansion (EPWE), which, in combination with experiments, have revealed the presence of so-called leaky channels at metal coordination sites (*11*). However, such 2D models neglect vertical modulations of the potential due to the intrinsic structure of molecular orbitals and their hybridization with the underlying substrate (*12*). This vertical interaction can substantially reshape the interfacial potential, underscoring the need for a more complete and realistic treatment of quantum confinement beyond idealized 2D approximations.

The crucial role of the third spatial dimension has not been uncovered so far as all existing studies have focused exclusively on the quantum confinement within the 2D free electron gas, associated with the so-called Shockley SS electrons of noble metal surfaces. The vertical distribution of these surface electrons with respect to the surface is described by their wave function or, more precisely, by their probability density given by the absolute square of the wave function. For typical noble metals such as Cu, Ag, or Au, the maximum probability density of the Shockley SS is localized within the first atomic layer of the surface (*13*) that is substantially lower than the adsorption height of molecular adsorbates or adatoms. Lateral confinement of these surface electrons within a 2D-MOPN can be modeled quantitatively by adjusting the parameters of the simplified surface potential model.

[1]Department of Physics and Research Center OPTIMAS, RPTU University Kaiserslautern-Landau, Erwin-Schrödinger-Straße 46, 67663 Kaiserslautern, Germany. [2]Experimentalphysik II, Institute of Physics, Augsburg University, D-86135 Augsburg, Germany. [3]School of Science, Hunan University of Technology, Zhuzhou 412007, China. [4]Physics Department, Faculty of Science, Al-Azhar University, Nasr City, E-11884 Cairo, Egypt. [5]Physics Department, Faculty of Science, Galala University, New Galala City, 43511 Suez, Egypt. [6]Centro de Física de Materiales CSIC/UPV-EHU-Materials Physics Center, 20018, San Sebastian, Spain. [7]IKERBASQUE, Basque Foundation for Science, Plaza Euskadi 5, 48009 Bilbao, Spain. [8]Physics Department E20, TUM School of Natural Sciences, Technical University of Munich, James-Franck-Straße 1, D-85748 Garching, Germany.
*Corresponding author. Email: lu.lyu@uni-a.de (L.L.); Benjamin.stadtmueller@uni-a.de (B.S.)

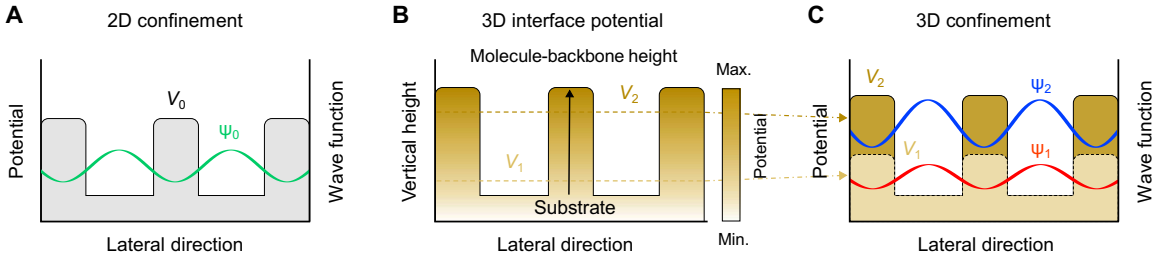

Fig. 1. Schematic illustration of different models for describing the quantum confinement of electrons in an organic porous network. (**A**) The currently established 2D confinement model considering a uniform lateral periodic potential V_0, neglecting the vertical potential variation. The confined electronic state ψ_0 (green) is located within the molecule-built potential wells. (**B**) Model of a 3D interface potential showing an increasing vertical potential from the substrate to the molecule-backbone height (black arrow). Darker shading indicates higher potential. The light and dark brown dashed lines mark potential levels $V_1 < V_2$ at different heights. (**C**) 3D confinement model incorporating both lateral and vertical potential variations. The vertical potential V_1 (light brown) and V_2 (dark brown), extracted from (B) (dashed arrows), produce a distinct vertical confinement for the electronic states ψ_1 (red) and ψ_2 (blue), respectively.

However, the confinement for Shockley SS is relatively weak, and the effective mass enhancement of the electrons is generally less than 60% (*9*, *14*). As a consequence, the contributions of molecular backbones and coordinating metal atoms to confinement potential are clearly underestimated in the idealized 2D model.

The Shockley SS is not the only type of SS that can be found on noble metal surfaces. Most famously, the surfaces can also host a Rydberg-like series of image-potential states (IPSs). Like Shockley SS electrons, IPSs are free electron–like states, but they are bound to the metal surface by the interaction of an excited electron just outside the metal surface and its induced image charge inside the substrate. This interaction leads to a sequence of unoccupied IPSs with a characteristic probability density maximum located ~3 to 5 Å above the surface (*15*), in notable contrast to the near-surface localization of the Shockley SS electrons. Recently, the confinement of IPSs has also been modeled through the utilization of 2D surface potentials (*16*).

To incorporate the effects of the modulation of the vertical potential, a 3D interface potential model, as illustrated in Fig. 1B, more accurately describes the spatial confinement of surface electrons in the 2D-MOPN on a metal substrate. In this model, the barrier potential of the molecular backbone is partially screened by the electron density of the underlying metallic substrate, resulting in a weaker barrier potential closer to the substrate. Consequently, the two vertical potential V_1 and V_2, located at different heights (dashed lines in Fig. 1B), produce a distinct confinement for the surface electronic states ψ_1 (red) and ψ_2 (blue), as illustrated in Fig. 1C. The simultaneous presence of Shockley SS and IPS, each exhibiting distinct vertical wave function distributions, thus provides a unique platform to explore the role of the third spatial dimension in SS quantum confinement.

In this work, we quantify the quantum confinement of both the Shockley SS and the first IPS ($n = 1$) within a Cu-T4PT (2,4,6-tri (4-pyridyl)-1,3,5-triazine) porous network on the (111) oriented copper surface. Using near-threshold and two-photon photoemission (2PPE) experiments in combination with momentum microscopy (*17*, *18*), we uncover a substantially different band structure for the Shockley SS and the IPS, indicative of fundamentally distinct quantum confinement behaviors. These experimental results are corroborated by density functional theory (DFT) calculations, which expose a pronounced contrast in the potential landscape at the vertical positions of the probability density maxima of the two SSs. This clear divergence underscores the crucial role of the vertical variation of the scattering potential landscape in the engineering of quantum confinement at surfaces.

RESULTS

The nanoporous architecture of the Cu-coordinated T4PT network

We begin by examining the structural and local electronic characteristics of the Cu-T4PT network. On the Cu(111) surface, the nitrogen ligands of T4PT molecules, bearing lone-pair sp^2 hybridized orbitals, spontaneously coordinate with native surface Cu atoms, leading to the self-assembly of a Cu-T4PT network. The large-scale STM and low-energy electron diffraction (LEED) measurements (Fig. 2A) highlight the formation of an almost perfect porous network with long-range order, exhibiting a 10 by 10 superlattice with a periodicity of 25.5 ± 0.2 Å along the $[\bar{1}01]$ and $[01\bar{1}]$ substrate directions. A molecular-resolution STM image (tip voltage bias $V_{tip} = +0.55$ eV; Fig. 2B) resolves the subtle structure of the pore. Each pore (~25 Å in diameter), surrounded by six T4PT molecules, displays both a central protrusion and a surrounding ring-like feature (green marks in the top). Previous studies of the Cu-T4PT system have shown the characterizations of scanning tunneling spectroscopy on the T4PT molecules, in which there are no contributions from molecule orbital–related interface states within the bias window of 0.55 eV below the Fermi level (*19*). Therefore, the observed STM signatures are the presence of in-pore standing waves arising from confined Shockley SS electrons scattered by the potential landscape of the Cu-T4PT network. These confined states manifest as well-defined peaks in the corresponding line profile (bottom). In addition, a distinct height difference in the local electronic density is observed between the two inequivalent T4PT molecules (labeled A and B) and are consistent with prior studies (*19*). This interpretation is supported by DFT calculations yielding the optimized Cu-T4PT network structure, shown in the left half of Fig. 2C. These calculations indicate that the network forms a mixed honeycomb-Kagome lattice according to the arrangements of the molecules and coordinating atoms. The neighboring molecules A and B, coordinated each with a Cu atom in a threefold symmetry, adsorb at different sites of the substrate (details in fig. S1). Furthermore, the DFT-based STM topography simulation (Fig. 2C, right half) shows an almost undetectable feature for the coordinated Cu center, indicating a low local electron density that aligns well with the experimental image in Fig. 2B.

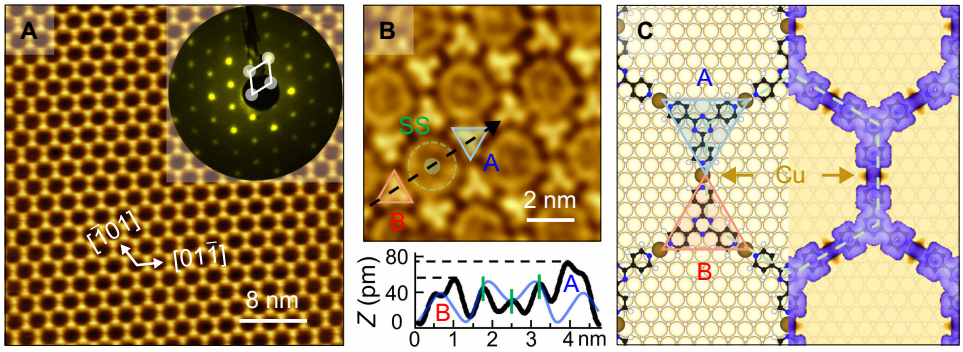

Fig. 2. Structure of the Cu-T4PT porous network on Cu(111). (**A**) Large-scale STM image (V_{tip} = +1.00 V) shows a well-ordered porous superlattice aligned along the surface [$\bar{1}$01] and [01$\bar{1}$] directions. The inset displays the corresponding LEED pattern (E_{kin} = 8 eV, inset), revealing a single-domain structure as indicated by the reciprocal-lattice spots (white). (**B**) The molecular-resolution STM image (top, V_{tip} = +0.55 V, i.e., for occupied states) shows central protrusion and a surrounding ring-like feature of the spatial confinement of Shockley SS electrons in the pores of the network structure. A line profile (bottom) along the dashed arrow crosses the Shockley SS features (green dashed circle and center spot) and T4PT molecules labeled as A and B (light blue and red triangles), showing a distinct height difference between A and B. The green bars highlight the positions of the confined Shockley SS. The blue curve illustrates the theoretically predicted electron distribution along the same direction within the nanopore (see the Supplementary Materials). (**C**) Simulation-optimized structural model (left side) of the Cu-T4PT network: Molecules A and B coordinated with a Cu metal atom. The corresponding simulated STM image (right side) is calculated for a constant current STM experiment at 0.55 eV below the Fermi level, with an isosurface density of 1.5 e Å^{-3}. All STM data were obtained at 106 K.

Shockley SS confinement in the Cu-T4PT porous network

The quantum confinement of both the Shockley SS and IPS in Cu-T4PT porous network, each exhibiting distinct vertical distributions, can be quantified by accessing their band dispersions using angle-resolved photoemission spectroscopy (ARPES) and momentum microscopy. In particular, the energy band shift, the electron effective mass, and the presence of new gaps at the Brillouin zone boundaries serve as characteristic signatures of quantum confinement. These experimentally accessible quantities allow gaining insight into the confinement strength of SSs in a 2D-MOPN (*8*, *14*).

We first focus on the confinement of the occupied Shockley SS, which can be addressed in near-threshold one-photon photoemission (1PPE) with a photon energy of 5.9 eV. Figure 3A presents the 3D momentum microscopy datacube (k_x, k_y, and E), in which two features with distinct parabolic dispersion are observed. The upper parabola, located near the Fermi energy ($E - E_F = 0$ eV), corresponds to the Shockley SS. The second feature at a larger binding energy arises from the so-called *sp*-*sp* Mahan cone (MC) transition, a well-known resonant bulk transition occurring only in the near-threshold photoemission regime for metals (*20*). This feature has been reported extensively (*21*–*24*) and does not play a further role for our discussion about surface electron confinement.

The momentum-resolved photoemission experimental data reveal clear signatures of the Shockley SS confinement within the Cu-T4PT porous network, in full agreement with our STM results shown in Fig. 2B. The constant energy map (CEM; Fig. 3B) at the Fermi energy displays periodic replicas of the ring-like Shockley SS emission pattern, arranged with a reciprocal lattice periodicity of $|\mathbf{k_a}| = |\mathbf{k_b}| = 0.28 \pm 0.01$ Å^{-1}. This periodicity matches the size of the surface Brillouin zone (BZ) defined by the Cu-T4PT superlattice. In other words, the centers of these Shockley SS replicas are localized at the $\overline{\Gamma}$-points of the superlattice BZs (marked by white hexagons). Replicated Shockley SS bands have previously been reported for the Cu-T4PT system (*25*). To address a more quantitative picture of the quantum confinement on the confined Shockley SS, we conducted additional ARPES experiments with a higher resolution. Instead of a broadband laser source, we used a monochromatized vacuum ultraviolet (VUV) excitation source ($h\nu = 21.2$ eV), and the corresponding data are shown in Fig. 3 (C to F). It is well established that the Shockley SS electrons behave as quasi-free electrons parallel to the surface, giving rise to a parabolic dispersion (*26*) described by $E(\mathbf{k}_{\parallel}) - E_F = E_0 + \frac{\hbar^2 k_{\parallel}^2}{2m^*}$, where E_F, E_0, m^*, and $k_{\parallel}$ denote the Fermi energy, band minimum energy, effective mass, and momentum wave vector parallel to the surface, respectively.

The ARPES intensity map with an energy-momentum relation in Fig. 3C displays the band structure of the confined Shockley SS for the Cu-T4PT network. The red arrow in Fig. 3B (BZ_1) marks the corresponding measurement location and direction in momentum space. It reveals a series of band replicas along the $\overline{\Gamma M}$-direction across the adjacent first and second BZs. A parabolic fit to the central band yields an effective mass of $m^* = 0.45\ m_0$ (m_0 is the free electron mass), which is almost identical to the reference value of $0.44m_0$ for the clean Cu(111) surface (Fig. 3D). The energy distribution curves (EDCs; Fig. 3E) reveal a downward shift of ~90 meV for the band bottom E_0 for the Cu-T4PT network. Organic molecules physisorbed on noble-metal surfaces are well known to induce a Pauli repulsion (push-back effect), which typically results in an upward shift of the Shockley SS toward the Fermi level (*9*, *27*), in clear contrast to the observation in our experiment. Instead, the observed downward shift is consistently explained by the presence of coordinated metal centers, which introduce an attractive potential and hybridize with the Shockley SS. Similar hybridization-induced downshifts of Shockley SS are also reported in other MOPNs formed with different molecular precursors (*11*, *28*).

The most crucial spectroscopic signature of quantum confinement–induced band renormalization is the opening of a weak bandgap (E_g) at the BZ boundary, which can be quantitatively assessed from ARPES measurements. However, the negligible increase in m^* suggests that E_g is small, indicating a relatively weak confinement effect

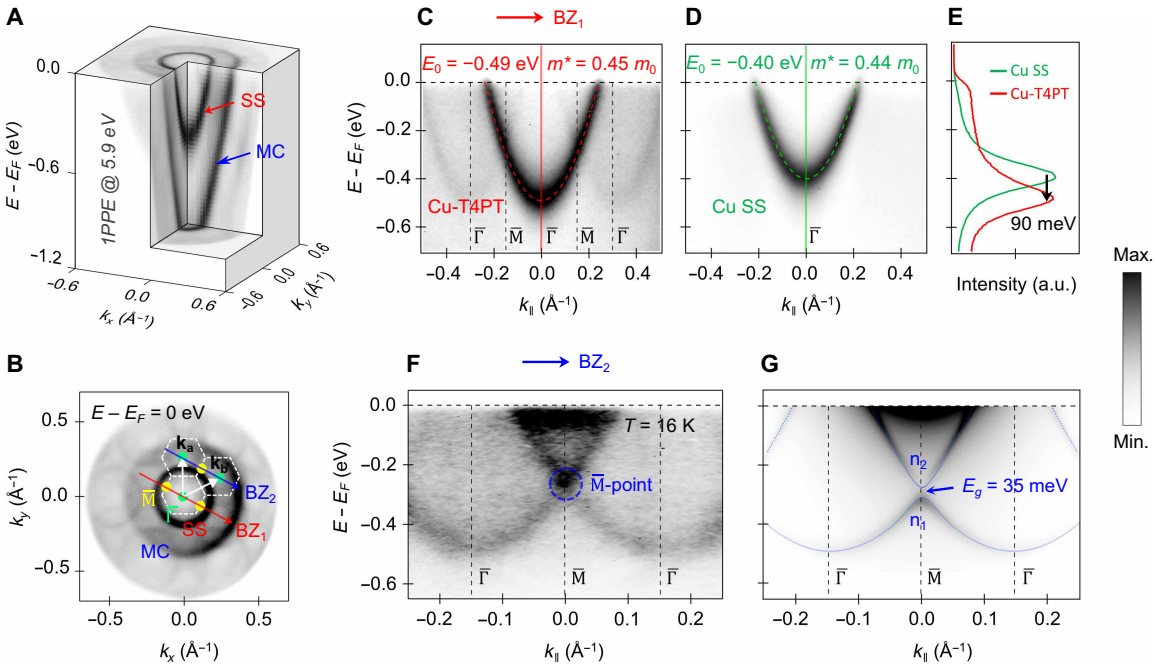

Fig. 3. Band dispersion of the Shockley SS in the Cu-T4PT porous network. (**A**) 3D photoemission intensity in energy-momentum space of the Cu-T4PT monolayer (ML) network on Cu(111), acquired using the 1PPE under grazing incidence illumination. The red and blue arrows indicate the Shockley SS and the MC structure, respectively. (**B**) Constant energy map (CEM) extracted from (A) at the Fermi level ($E - E_F = 0$ eV) revealing replicas of the Shockley SS, with a reciprocal lattice vector of $|\mathbf{k_a}| = |\mathbf{k_b}| = 0.28 \pm 0.01$ Å^{-1}. White dashed hexagons delineate the first and second Brillouin zones (BZs) of the Cu-T4PT network. High-symmetry points $\overline{\Gamma}$ and $\overline{\mathrm{M}}$ are marked with light green and yellow dots, respectively. (**C** and **D**) ARPES data measured along the red arrow in (B) (BZ_1) for the Cu-T4PT network and Cu(111) surface. Band parameters E_0 (band bottom energy) and m^* (electron effective mass) are extracted from fitting the Shockley SS intensity with a parabolic dispersion (red and green dashed curves). (**E**) Energy-distribution curves extracted at the $\overline{\Gamma}$-point (red and green lines) in (C) and (D), highlighting a 90-meV downward shift of E_0 upon the formation of the Cu-T4PT network. (**F**) ARPES map recorded at $T = 16$ K along the blue arrow in (B) (BZ_2) for the Cu-T4PT network, revealing a distinct intensity contrast above and below the $\overline{\mathrm{M}}$-point. (**G**) EPWE simulations reproduce the Shockley SS bands in (F) and predict a bandgap of $E_g = 35$ meV, with quantized states n_1 and n_2 above and below the gap point. Data in (A) and (B) were recorded with *p*-polarized laser light ($h\nu = 5.9$ eV). Data in (C) to (F) were acquired with VUV light ($h\nu = 21.2$ eV). (A) to (E) were measured at room temperature. a.u., arbitrary units.

exerted by the Cu-T4PT network. Moreover, the very strong photoemission intensity of the Shockley SS in the first BZ (high photoemission cross section) obscures any visible gap signatures near the $\overline{\mathrm{M}}$-points in Fig. 3C. To circumvent these limitations, we recorded an additional ARPES dataset at a low temperature ($T = 16$ K) for the Cu-T4PT network, along a momentum cut through two adjacent second BZs, as indicated by the blue arrow in Fig. 3B (BZ_2). The ARPES map in Fig. 3F reveals the dispersion of two Shockley SS bands in neighboring BZs with almost identical spectral yield. Both bands display a characteristic intensity contrast at the crossing $\overline{\mathrm{M}}$-point above and below the energy of $E - E_F = -0.30$ eV, providing the evidence of a small E_g at the BZ boundary. This experimental observation is supported by EPWE simulations shown in Fig. 3G. The calculated Shockley SS dispersion using a 2D surface potential model of the Cu-T4PT reproduces the key features of the experimental data, corroborating a bandgap of $E_g = 35$ meV at the $\overline{\mathrm{M}}$-point. Further EPWE simulations (fig. S2) reveal two discrete Shockley SS eigenstates below the Fermi level, whose corresponding spatial local density of states maps exhibit distinctly different distributions within the nanopores: a dome-like central protrusion and a ring-like structure. These features are consistent with the standing-wave patterns observed in STM (Fig. 2B). Owing to the energy-integrated nature of constant-current STM measurements, the experimentally observed STM contrast represents a superposition of contributions from multiple discrete Shockley SS eigenstates, giving rise to the simultaneous appearance of both features. For direct comparison, the sum of the EPWE-simulated line profiles of the two discrete Shockley SS eigenstates (fig. S2, E and F) is overlaid onto the experimental STM line profile in Fig. 2B. The slightly reduced prominence of the central feature in the simulated curve originates from the broadening of the central eigenstate in the EPWE simulation.

First IPS ($n = 1$) confinement in the Cu-T4PT porous network

We now turn to the quantum confinement of the IPS electrons in the Cu-T4PT network, which exhibit substantially different vertical probability density distributions compared to the Shockley SS electrons. Owing to their excited-state character, IPSs cannot be probed in the same linear photoemission experiment as the Shockley SS. Moreover, the high excitation energies of IPSs (close to the vacuum level), together with the fragility of metal-organic coordination bonds, strongly limit the applicability of high-bias STS to such systems. We therefore use 2PPE experiments. 2PPE has been experimentally and theoretically established as a quantitative method for probing IPSs on various material systems (*29*–*31*), providing direct energy- and momentum-resolved access to unoccupied states above the Fermi level. In this approach, we use the second harmonic of a titanium-sapphire (Ti:Sa) laser oscillator with a photon energy of

3.44 eV. Absorption of a photon from the laser pulse excites an electron from the occupied states into the intermediate IPS. A second photon from the same pulse subsequently photoionizes the electron into the vacuum as illustrated in Fig. 4A. By resolving the energy and momentum of the emitted photoelectrons, we obtain momentum space signatures of the initial state (|i⟩), intermediate state (|j⟩), and final state (|f⟩) simultaneously, enabling a quantitative measurement of the band dispersion of the IPSs.

The corresponding 2PPE measurements are presented in Fig. 4 (B to G). The CEM in Fig. 4B, taken near the vacuum level ($E - E_F =$ 3.25 eV), reveals again clear ring-like features indicative of periodic replicas of the IPS emission pattern in each surface BZ of the Cu-T4PT superlattice. This is very similar to the replicas of the Shockley SS observed in Fig. 3B and thus points to a quantum confinement of the excited IPS electrons. A more quantitative view onto the IPS band dispersion can again be obtained with additional ARPES experiments in the 2PPE regime. Similar to Shockley SS electrons, IPS electrons exhibit a free electron–like parabolic dispersion near the vacuum level, which follows a Rydberg-like series: $E - E_F = E_{vac} - \frac{0.85\ eV}{(n+a)^2} + \frac{\hbar^2 k_\parallel^2}{2m^*}$, where E_{vac} is the vacuum level energy, n is the image state index, and a is the quantum defect parameter related to the bulk band structure (*32*). The ARPES intensity map in Fig. 4C, recorded along the red arrow in Fig. 4B (BZ_1), clearly shows two parabolic bands with substantially different curvatures corresponding to the Shockley SS and the first IPS. The Shockley SS band matches the dispersion observed in the linear photoemission experiment (Fig. 3C). It is visible in our 2PPE data due to a direct two–photo-ionization process via virtual transition from the occupied Shockley SS to the vacuum (*33*). In contrast, the IPS band appears as very flat with its band bottom energy (E_0) located 3.18 eV relative to E_F, despite being a free electron–like SS. A parabolic fit to the IPS band yields an effective mass of $m^*_{IPS\_Cu-T4PT} = 2.07\ m_0$, which is approximately 2.6 times larger than the value for the pristine Cu(111) ($m^*_{IPS\_Cu} = 0.81\ m_0$; see fig. S3). Moreover, the IPS band bottom E_0 shifts toward E_F by 0.77 eV compared to the clean Cu(111) and is now located deeper in the L-bandgap of the substrate.

This exceptionally large increase in the effective mass of the IPS band provides a direct signature of strong quantum confinement of the IPS electrons within the 3D interface potential landscape of the Cu-T4PT network and not caused by the adsorption-induced band shift of the IPS. To further support this conclusion, we monitored the effective mass of the IPS on clean Cu(111) at different band bottom positions through doping the surface with potassium (K) atoms. Here, gentle charge doping induces a continuous downward shift of the IPS

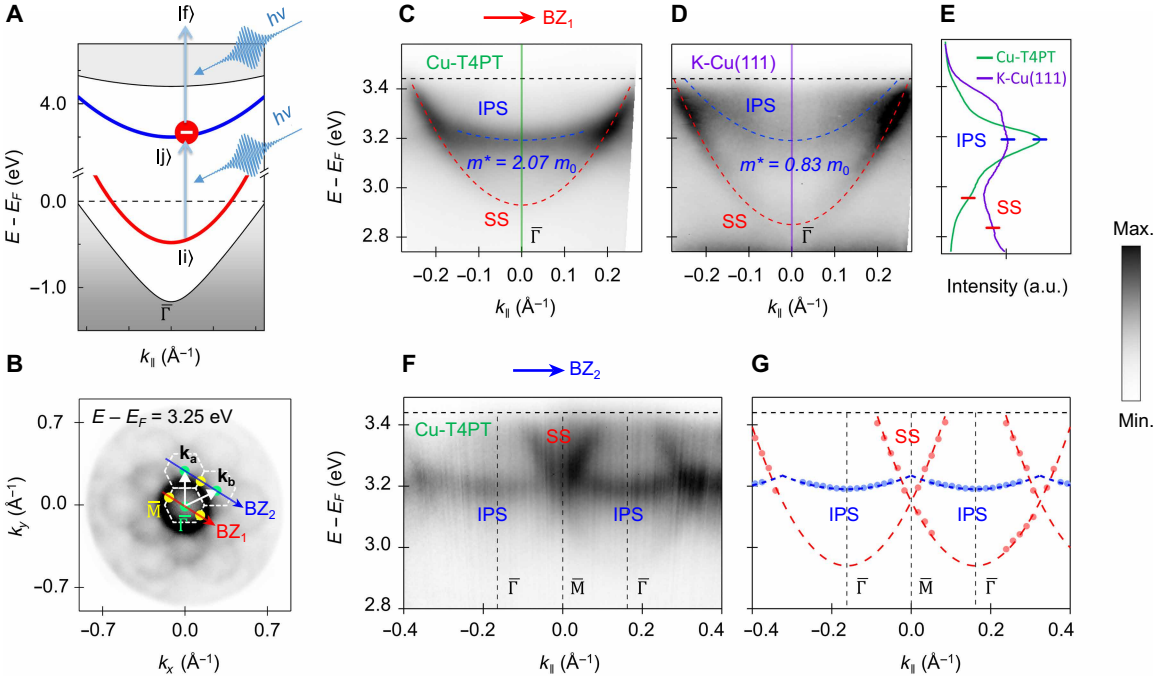

Fig. 4. Band structure of the first IPS ($n = 1$) in the Cu-T4PT porous network. (**A**) Schematic illustration of the one-color 2PPE process used to probe unoccupied states above the Fermi level. One photon of the pulse excites electrons from an occupied initial state |i⟩ into an unoccupied intermediate state |j⟩, which is further promoted to the final state |f⟩ above the vacuum level via a subsequent absorption of another photon of the same pulse. (**B**) CEM at an intermediate state energy of $E - E_F = 3.25$ eV, showing ring-like replicas of the unoccupied first IPS bands with a reciprocal lattice periodicity of $|\mathbf{k_a}| = |\mathbf{k_b}| = 0.28 \pm 0.02$ Å^{-1}. The white dashed hexagons mark the first and second BZs of the Cu-T4PT lattice. High-symmetry points $\bar{\Gamma}$ and $\bar{M}$ are marked with light green and yellow dots, respectively. (**C** and **D**) ARPES band dispersions recorded along the red arrow (BZ_1) for the Cu-T4PT network and for the Cu(111) surface doped with a fraction of a ML (0.3 ML) of potassium [K-Cu(111)]. The blue and red parabolas indicate the fit of the band dispersion for the IPS and the Shockley SS, respectively. (**E**) Energy-distribution curves (EDCs) extracted at the $\bar{\Gamma}$-point (green and purple lines) from (C) and (D), highlighting an identical IPS energy (band bottom positions) of $E_0 - E_F = 3.18$ eV. (**F**) ARPES intensity map measured along the blue arrow in (B) (BZ_2) for the Cu-T4PT network, showing two practically flat IPS bands from adjacent second BZs that intersect at the $\bar{M}$-point. (**G**) Extracted band positions (solid dots) from (F), overlaid with parabolic fits for the IPS (blue) and Shockley SS (red) bands. All measurements were performed at room temperature using a *p*-polarized laser with a photon energy of $h\nu = 3.44$ eV.

energy due to the lowering of the surface work function. Upon deposition of 0.3 monolayers (ML) of K-atoms, the IPS band on the K-doped Cu(111) surface in Fig. 4D shifts to the same energy position as the one observed for the Cu-T4PT network, as confirmed by the additional EDC curves (Fig. 4E). However, its effective mass is only $m^*_{IPS} = 0.83\ m_0$ and thus identical to the one of the undoped surface. This observation unambiguously demonstrates a negligible change in the coupling of the IPS state with the Cu bulk bands upon lowering the IPS into the *L*-bandgap. Further insight is provided by additional ARPES measurements on the Cu-T4PT network along the direction marked with a blue arrow (BZ_2) in Fig. 4B. The map, shown in Fig. 4F, reveals a remarkably flat first IPS band entirely residing within the Cu bulk bandgap. The extracted band positions (method in fig. S4) plotted in Fig. 4G clearly demonstrate that the first IPS band in the Cu-T4PT network has a periodic and quantized dispersion structure.

In this regard, our experimental results not only show that optically excited IPS electron can also be confined in a 2D-MOPN, but the comparative analysis between Shockley SS and IPS confinement within the same material system highlights a notable dependence of quantum confinement strength on the vertical wave function distribution of the Shockley SS. This underlines the crucial role of the vertical component of the 3D interface potential landscape in governing the quantum confinement of SS electrons.

DISCUSSION

The microscopic origin of the notably contrasting quantum confinement behaviors for the Shockley SS and the IPS can be elucidated through ab initio DFT calculations of the Cu-T4PT network (see Materials and Methods for details). A fully relaxed and optimized model of the porous network is shown in Fig. 5A, in which each Cu adatom is coordinated by two adjacent T4PT molecules.

The local interactions among the molecules, the Cu atom, and the substrate induce a characteristic charge redistribution at the Cu coordination site, which is clearly illustrated in the charge density difference plot in Fig. 5B. Notably, a distinct charge depletion is found at the position of the Cu adatoms (blue region), accompanied by a charge accumulation barely underneath (red region), which coincides with the formation of the downward electric fields ($\vec{E}$) and the upward dipole ($\vec{D}$) at the Cu site. These local surface (or interfacial) dipoles can substantially reduce the work function (*34*) and lower the vacuum level by 0.85 eV (see fig. S5). Consequently, the energy position of the IPS shifts deeper in the *L*-bandgap of the Cu substrate, consistent with the experimentally observed energy shifts (more parameters summarized in table S1).

The local charge redistribution, including the charge transfer processes within the porous network structure, reflects the interfacial hybridization and thereby reshapes the 3D interface potential landscape responsible for the confinement of both Shockley SS and IPS electrons. To figure out the impact of the vertical modulation of this potential, we evaluated the vertical electrostatic potential (ESP) landscapes (Fig. 5C) perpendicular to the Cu(111) surface, extracted along two representative directions ("*H*" and "*L*" marked in Fig. 5A): through the Cu coordination sites (left) and the molecular backbones (right). Overall, both potential landscapes exhibit a predominantly repulsive electron potential (blue regions) in both the T4PT molecules and Cu atoms, which is

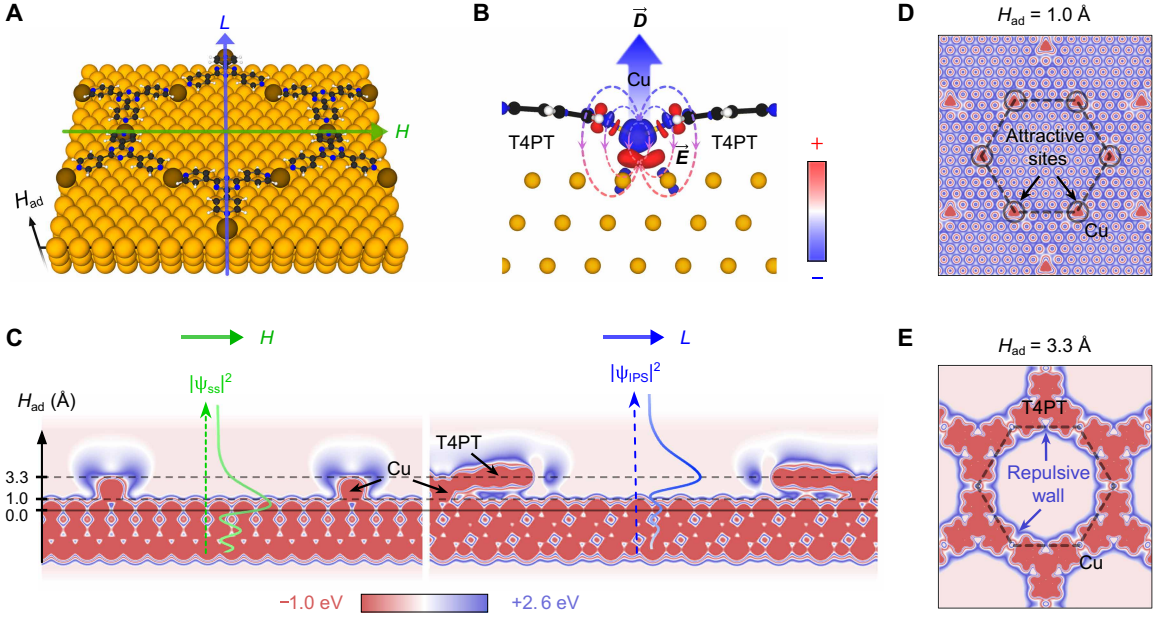

Fig. 5. 3D potential landscape in the Cu-T4PT porous network. (**A**) Top view of the Cu-T4PT structure on the Cu(111) surface. The horizontal (*H*, green) and longitudinal (*L*, blue) directions correspond to axes across the coordinated Cu atoms (brown spheres) and T4PT molecules, respectively. (**B**) Side view of the charge density difference plot at one Cu-T4PT coordination site. Red (charge accumulation) and blue (charge depletion) regions indicate downward pointing electric fields ($\vec{E}$, dashed lines) and an upward pointing interfacial dipole ($\vec{D}$, blue arrow). (**C**) Simulated electrostatic potential (ESP) maps along cross-sections of the *H* (left) and the *L* (right) directions, as marked in (A). The vertical adsorption heights (H_{ad}) of 1.0 and 3.3 Å, measured from the top Cu layer (H_{ad} = 0.0 Å), correspond to the average height of the Cu surface and T4PT backbones, respectively. The blue and red areas represent repulsive and attractive potential, respectively. Model curves within the pore illustrate the vertical probability distribution of the Cu(111) Shockley SS (green) and the first IPS (blue). (**D**) Planar ESP map at H_{ad} = 1.0 Å highlights attractive potential sites at coordinated Cu atoms. (**E**) Planar ESP map at H_{ad} = 3.3 Å reveals a sealed repulsive potential wall surrounding the Cu-T4PT pores. Isosurface values in (B): ±0.004 e $Å^{-3}$.

consistent with the existence of quantum wells for surface electrons in the Cu-T4PT network pores. However, on closer inspection, we find characteristics of strong repulsive potential residing at the vicinity of the T4PT molecule for the average adsorption height of its backbone, while the Cu sites only show a repulsive potential at large surface distances (H_{ad}, ~3 Å) and an attractive potential very close to the surface (H_{ad}, ~1 Å). These distinct vertical potential distributions are consistent with the schematic 3D interface potential model (Fig. 1B) and account for the notably different confinement strengths of the Shockley SS and the IPS electrons. We illustrate this by sketching the vertical probability density of the Cu(111) Shockley SS ($|\psi_{SS}|^2$) and first IPS ($|\psi_{IPS}|^2$) in Fig. 5C. Most of the Shockley SS density is located very close to the metal surface (peak ~1 Å), where it overlaps with the attractive region near the Cu sites. This behavior is further illustrated by the 2D ESP map in Fig. 5D (extracted at a vertical height $H_{ad} = 1$ Å). The attractive sites of the Cu atoms act as leaky channels for the Shockley SS electrons, weakening the lateral confinement and explaining the limited band renormalization observed in ARPES. Although the Cu-T4PT network provides an identical lateral barrier geometry for both Shockley SS and IPS scattering, the two states exhibit fundamentally different vertical wave function distributions and ESP landscapes. As a result, the effective scattering potentials associated with the molecular blocks and the coordinated metal atoms are intrinsically different for the Shockley SS and the IPS within the same system.

In contrast, the IPS electrons are predominantly located at a vertical position of ~3.3 Å, coinciding with the adsorption height of the T4PT molecules. At this height, our calculation in Fig. 5B reveals no signatures of short-range hybridization-induced charge redistribution, in contrast to the situation close to the Cu surface. Instead, the peripheries of the T4PT backbones and the coordinating Cu atoms form a sealed and almost ring-like repulsive potential wall around each pore as shown in the 2D ESP map (Fig. 5E). Owing to the pronounced spatial and energetic mismatch between the IPS wave function (an excited state located more than 3 eV above the Fermi energy) and the Cu-T4PT network, the formation of leaky channels is strongly suppressed. Consequently, the combination of a strongly repulsive potential at the adsorption height of the network components with the absence of any leaky channels at the same vertical position is responsible for the stronger confinement of the IPS electrons within the Cu-T4PT porous network and thus for the formation of an almost flat IPS band by the quantum confinement.

In conclusion, our work demonstrates the pivotal role of the 3D interface potential landscape for the quantum confinement of different types of surface electrons in porous nanostructures. By systematically examining both Shockley SS and IPS, each with distinct vertical electron density distributions, we uncover notable disparities in band dispersion and effective mass renormalization within a Cu-coordinated T4PT porous network. These differences arise from vertical potential variations: Leaky channels at Cu sites close to the surface result in a weak confinement of the Shockley SS, whereas a strong, sealed repulsive potential at the adsorption height of the molecular backbones leads to a giant confinement of the IPS electrons. The comparison highlights that effective confinement of SSs within MOPNs requires consideration of both lateral and vertical components of the interface potential. The lateral potential is governed by the barrier geometry (size, width, and structural symmetry) of the network, whereas the vertical potential is strongly dependent on the adsorption height of the network and the interaction strength with the substrate. Our results demonstrate a general concept for 3D potential landscape. It is thus not limited to Shockley SSs and IPSs but can be extended to other types of states, such as hybrid interface or charge transfer states, as long as they can be confined in the nanopores by backscattering at the surface potential.

Our findings establish a pronounced expanded framework for engineering quantum confinement by harnessing the full 3D complexity of surface potential landscapes. This advancement represents a critical leap forward, enabling the simultaneous and selective confinement of multiple SSs within individual nanopores. By achieving this level of control, we open the door to realizing coherent quantum interference and superposition of SSs in artificial nanostructures, key prerequisites for the development of robust quantum computing architectures and next-generation nanoscale quantum technologies.

MATERIALS AND METHODS

Sample preparation

All experiments were carried out in two commercial ultrahigh-vacuum systems (base pressure ~ 10^{-10} mbar): a SPECS GmbH ARPES setup and an in situ multichamber Omicron variable-temperature STM, the latter integrated with a FOCUS GmbH PEEM chamber. The Cu(111) substrate (MaTecK) was cleaned through multiple cycles of Ar-ion sputtering (1.0 to 1.8 kV) and annealing (610° to 650°C). T4PT molecules (Tokyo Chemical Industry Co., Ltd. (TCI), purity > 97%) were thermally evaporated at 450 K with a deposition rate of 0.33 ML·min^{-1} [1 ML = full ML Cu-T4PT network on Cu(111)]. After deposition, the T4PT film was annealed at 410 K for 30 min to form a defect-free Cu-coordinated T4PT network. Potassium atoms (SAES Getters) were deposited at a rate of 0.07 ML·min^{-1} on clean Cu(111). During all depositions, substrates were held at room temperature.

Scanning tunneling microscopy

STM measurements were performed at 106 K (liquid nitrogen cooling) in constant current mode, using a tunneling current (I_t) of 70 to 90 pA. The bias voltage (V_{tip}) is applied to the STM tip, and the positive and negative values correspond to tunneling into the samples' occupied and unoccupied states, respectively. All STM images were processed using the open source software Gwyddion (*35*).

Momentum microscopy

Momentum-resolved photoemission measurements were performed using a photoemission electron microscope (FOCUS PEEM) combined with a time-of-fight delay-line detector. 3D datasets (k_x, k_y, and E_{kin}) were acquired with energy and momentum resolutions better than $\Delta E < 100$ meV and $\Delta k < 2 \times 10^{-2}$ Å, respectively. The excitation sources included the third (THG, $h\nu = 4.6$ eV) and fourth (FHG, $h\nu = 5.9$ eV) harmonics of a commercial pulsed titanium-sapphire (Ti:Sa) laser (Tsunami, Spectra-Physics, central wavelength of 840 nm), with nonlinear conversion achieved using a THG Tripler-Box and a beta-barium borate (BBO) crystal, respectively. For the 2PPE experiments, the second harmonic (SHG, $h\nu = 3.44$ eV) from a separate femtosecond Ti:Sa laser (Mai Tai, Spectra-Physics, central wavelength of 720 nm) was used. The samples were illuminated with linearly *p*-polarized light under grazing incidence (65°) relative to the surface normal direction.

Angle-resolved photoemission spectroscopy

ARPES spectra were acquired using a hemispherical energy analyzer (PHOIBOS 150, SPECS) equipped with a charge-coupled device detector. The energy and momentum resolutions were better than

5 meV and 1×10^{-2} Å^{-1}, respectively. 1PPE measurements were performed using a monochromatic He Iα discharge lamp (21.2 eV, Scienta VUV 5K). For the 2PPE experiments, we used the same laser source (Mai Tai, Spectra-Physics) and SHG at $h\nu = 3.44$ eV, as mentioned above. The incidence angle of the *p*-polarized laser beam is 45° relative to the normal direction of the surface. A sample bias voltage of −4 V was applied to the measurements, and the distortion of low-kinetic photoelectrons was corrected (*36*) considering the sample-detector potential differences. The cooling measurement at 16 K was conducted by liquid helium.

EPWE simulations

EPWE was performed using the code developed by Javier Garcia de Abajo, widely applied in the study of 2D electron gas scattering in periodic nanostructures with arbitrarily shaped barriers (*6*, *37*). Within this code, muffin-tin potentials are assigned to the regions of molecule (V_1) and substrate (V_0). The wave function is expressed as a linear combination of plane waves, and the central form of the Schrödinger equation is solved to obtain the energy eigenvalues and wave functions across all momentum values. A 10 by 10 reciprocal lattice corresponding to 100 plane waves was used to ensure satisfactory convergence in the Fourier expansion of the potential. EPWE was used to calculate the band structures, density of states, and photoemission maps for Shockley SS confinement within the Cu-T4PT porous network.

Ab initio calculations

DFT calculations were carried out with the Vienna Ab initio Simulation Package (VASP) code (*38*). The projected augmented wave method (*39*) was used with a plane-wave cutoff of 400 eV. The electron-exchange correlation was treated using the generalized gradient approximation with the Predew-Burke-Ernzerhof function (*40*). In addition, the nonlocal exchange-correlation function of optB86b + van der Waals (vdW) (*41*) was included for van der Waals interactions. A supercell slab of the Cu-T4PT system contains three Cu(111) layers, two T4PT molecules, and three coordinated Cu atoms, with a vacuum gap of 15 Å in the *z* direction. All atomic positions were relaxed with a force tolerance below 0.02 eV/Å. Only the Γ-point was sampled in the geometry optimization. STM simulations were based on the Tersoff-Hamann approximation (*42*), and the charge density contour was generated as constant-current images in P4VASP. For the optimized Cu-T4PT structure, the spatial ESP map was calculated using the VASP code, considering only the Hartree potential contributions. All structural visualizations were created using VESTA (*43*).

Supplementary Materials

This PDF file includes:

Supplementary Text
Figs. S1 to S5
Table S1

REFERENCES

1. M. F. Crommie, C. P. Lutz, D. M. Eigler, Confinement of electrons to quantum corrals on a metal surface. *Science* **262**, 218–220 (1993).
2. N. N. Negulyaev, V. S. Stepanyuk, L. Niebergall, P. Bruno, W. Hergert, J. Repp, K. H. Rieder, G. Meyer, Direct evidence for the effect of quantum confinement of surface-state electrons on atomic diffusion. *Phys. Rev. Lett.* **101**, 226601 (2008).
3. L. Yan, P. Liljeroth, Engineered electronic states in atomically precise artificial lattices and graphene nanoribbons. *Adv. Phys. X* **4**, 1651672 (2019).
4. E. J. Heller, M. F. Crommie, C. P. Lutz, D. M. Eigler, Scattering and absorption of surface electron waves in quantum corrals. *Nature* **369**, 464–466 (1994).
5. H. C. Manoharan, C. P. Lutz, D. M. Eigler, Quantum mirages formed by coherent projection of electronic structure. *Nature* **403**, 512–515 (2000).
6. I. Piquero-Zulaica, J. Lobo-Checa, Z. M. A. El-Fattah, J. E. Ortega, F. Klappenberger, W. Auwärter, J. V. Barth, Engineering quantum states and electronic landscapes through surface molecular nanoarchitectures. *Rev. Mod. Phys.* **94**, 045008 (2022).
7. L. Dong, Z. A. Gao, N. Lin, Self-assembly of metal-organic coordination structures on surfaces. *Prog. Surf. Sci.* **91**, 101–135 (2016).
8. J. Lobo-Checa, M. Matena, K. Müller, J. H. Dil, F. Meier, L. H. Gade, T. A. Jung, M. Stöhr, Band formation from coupled quantum dots formed by a nanoporous network on a copper surface. *Science* **325**, 300–303 (2009).
9. I. Piquero-Zulaica, J. Lobo-Checa, A. Sadeghi, Z. M. Abd El-Fattah, C. Mitsui, T. Okamoto, R. Pawlak, T. Meier, A. Arnau, J. E. Ortega, J. Takeya, S. Goedecker, E. Meyer, S. Kawai, Precise engineering of quantum dot array coupling through their barrier widths. *Nat. Commun.* **8**, 787 (2017).
10. N. Kepčija, T.-J. Huang, F. Klappenberger, J. V. Barth, Quantum confinement in self-assembled two-dimensional nanoporous honeycomb networks at close-packed metal surfaces. *J. Chem. Phys.* **142**, 101931 (2015).
11. I. Piquero-Zulaica, A. Sadeghi, M. Kherelden, M. Hua, J. Liu, G. Kuang, L. Yan, J. E. Ortega, Z. M. A. El-Fattah, B. Azizi, N. Lin, J. Lobo-Checa, Electron transmission through coordinating atoms embedded in metal-organic nanoporous networks. *Phys. Rev. Lett.* **123**, 266805 (2019).
12. M. Willenbockel, D. Lüftner, B. Stadtmüller, G. Koller, C. Kumpf, S. Soubatch, P. Puschnig, M. G. Ramsey, F. S. Tautz, The interplay between interface structure, energy level alignment and chemical bonding strength at organic–metal interfaces. *Phys. Chem. Chem. Phys.* **17**, 1530–1548 (2015).
13. M. G. Vergniory, J. M. Pitarke, S. Crampin, Lifetimes of Shockley electrons and holes at Cu(111). *Phys. Rev. B* **72**, 193401 (2005).
14. I. Piquero-Zulaica, Z. M. A. El-Fattah, O. Popova, S. Kawai, S. Nowakowska, M. Matena, M. Enache, M. Stöhr, A. Tejeda, A. Taleb, E. Meyer, J. E. Ortega, L. H. Gade, T. A. Jung, J. Lobo-Checa, Effective determination of surface potential landscapes from metal-organic nanoporous network overlayers. *New J. Phys.* **21**, 053004 (2019).
15. E. V. Chulkov, V. M. Silkin, P. M. Echenique, Image potential states on metal surfaces: Binding energies and wave functions. *Surf. Sci.* **437**, 330–352 (1999).
16. J. Deyerling, I. Piquero-Zulaica, M. A. Ashoush, K. Seufert, M. A. Kher-Elden, Z. M. Abd El-Fattah, W. Auwärter, Formation of an extended quantum dot array driven and autoprotected by an atom-thick h-BN Layer. *ACS Nano* **17**, 5448–5458 (2023).
17. B. Krömker, M. Escher, D. Funnemann, D. Hartung, H. Engelhard, J. Kirschner, Development of a momentum microscope for time resolved band structure imaging. *Rev. Sci. Instrum.* **79**, 053702 (2008).
18. F. Haag, T. Eul, P. Thielen, N. Haag, B. Stadtmüller, M. Aeschlimann, Time-resolved two-photon momentum microscopy—A new approach to study hot carrier lifetimes in momentum space. *Rev. Sci. Instrum.* **90**, 103104 (2019).
19. T. R. Umbach, M. Bernien, C. F. Hermanns, L. L. Sun, H. Mohrmann, K. E. Hermann, A. Krüger, N. Krane, Z. Yang, F. Nickel, Y. M. Chang, K. J. Franke, J. I. Pascual, W. Kuch, Site-specific bonding of copper adatoms to pyridine end groups mediating the formation of two-dimensional coordination networks on metal surfaces. *Phys. Rev. B* **89**, 235409 (2014).
20. G. D. Mahan, Theory of photoemission in simple metals. *Phys. Rev. B* **2**, 4334–4350 (1970).
21. E. D. Hansen, T. Miller, T. C. Chiang, Surface photoemission in Ag(100). *Phys. Rev. B* **55**, 1871–1875 (1997).
22. A. Winkelmann, V. Sametoglu, J. Zhao, A. Kubo, H. Petek, Angle-dependent study of a direct optical transition in the *sp* bands of Ag(111) by one- and two-photon photoemission. *Phys. Rev. B* **76**, 195428 (2007).
23. A. Winkelmann, A. Akin Ünal, C. Tusche, M. Ellguth, C.-T. Chiang, J. Kirschner, Direct *k*-space imaging of Mahan cones at clean and Bi-covered Cu(111) surfaces. *New J. Phys.* **14**, 083027 (2012).
24. T. Eul, J. Braun, B. Stadtmüller, H. Ebert, M. Aeschlimann, Spectroscopic evidence for a new type of surface resonance at noble-metal surfaces. *Phys. Rev. Lett.* **127**, 196405 (2021).
25. C.-S. Zhou, X.-R. Liu, Y. Feng, X. Shao, M. Zeng, K. Wang, M. Feng, C. Liu, Quantum-confinement-induced periodic surface states in two-dimensional metal-organic frameworks. *Appl. Phys. Lett.* **117**, 191601 (2020).
26. S. Kevan, R. Gaylord, High-resolution photoemission study of the electronic structure of the noble-metal (111) surfaces. *Phys. Rev. B* **36**, 5809–5818 (1987).
27. L. Lyu, J. Xiao, Z. M. A. El-Fattah, T. Eul, M. Ashoush, J. He, W. Yao, I. Piquero-Zulaica, S. Mousavion, B. Arnoldi, S. Becker, J. V. Barth, M. Aeschlimann, B. Stadtmüller, Temperature-driven confinements of surface electrons and adatoms in a weakly interacting 2D organic porous network. arXiv:2307.06808 [cond-mat.mtrl-sci] (2023).
28. I. Piquero-Zulaica, J. Li, Z. M. Abd El-Fattah, L. Solianyk, I. Gallardo, L. Monjas, A. K. H. Hirsch, A. Arnau, J. E. Ortega, M. Stöhr, J. Lobo-Checa, Surface state tunable

energy and mass renormalization from homothetic quantum dot arrays. *Nanoscale* **11**, 23132–23138 (2019).
29. T. Fauster, W. Steinmann, Two-photon photoemission spectroscopy of image states. *Electromagnetic Waves* **2**, 347–411 (1995).
30. K. Ishioka, C. Gahl, M. Wolf, Femtosecond dynamics of image potential states of C6F6/Cu (111) studied with two-photon photoemission. *Surf. Sci.* **454**, 73–77 (2000).
31. M. Machado, E. Chulkov, V. Silkin, U. Höfer, P. Echenique, Electron lifetimes in image-potential states at metal–dielectric interfaces. *Prog. Surf. Sci.* **74**, 219–237 (2003).
32. P. Echenique, J. Pitarke, E. Chulkov, V. Silkin, Image-potential-induced states at metal surfaces. *J. Electron Spectros. Relat. Phenomena* **126**, 163–175 (2002).
33. H. Ueba, T. Mii, Theory of energy- and time-resolved two-photon photoemission from metal surfaces—Influence of pulse duration and excitation condition. *Appl. Phys. A* **71**, 537–545 (2000).
34. R. W. Verhoef, M. Asscher, The work function of adsorbed alkalis on metals revisited: A coverage-dependent polarizability approach. *Surf. Sci.* **391**, 11–18 (1997).
35. D. Nečas, P. Klapetek, Gwyddion: An open-source software for SPM data analysis. *Centr. Eur. J.Phys.* **10**, 181–188 (2012).
36. M. Hengsberger, F. Baumberger, H. Neff, T. Greber, J. Osterwalder, Photoemission momentum mapping and wave function analysis of surface and bulk states on flat Cu(111) and stepped Cu(443) surfaces: A two-photon photoemission study. *Phys. Rev. B* **77**, 085425 (2008).
37. Z. Abd El-Fattah, M. Kher-Elden, I. Piquero-Zulaica, F. G. de Abajo, J. E. Ortega, Graphene: Free electron scattering within an inverted honeycomb lattice. *Phys Rev B* **99**, 115443 (2019).
38. G. Kresse, J. Furthmüller, Efficiency of ab-initio total energy calculations for metals and semiconductors using a plane-wave basis set. *Comput. Mater. Sci.* **6**, 15–50 (1996).
39. P. E. Blöchl, Projector augmented-wave method. *Phys. Rev. B* **50**, 17953–17979 (1994).
40. J. P. Perdew, K. Burke, M. Ernzerhof, Generalized gradient approximation made simple. *Phys. Rev. Lett.* **77**, 3865–3868 (1996).
41. J. Klimeš, D. R. Bowler, A. Michaelides, Van der Waals density functionals applied to solids. *Phys. Rev. B* **83**, 195131 (2011).
42. J. Tersoff, D. R. Hamann, Theory of the scanning tunneling microscope. *Phys. Rev. B* **31**, 805–813 (1985).
43. K. Momma, F. Izumi, VESTA 3 for three-dimensional visualization of crystal, volumetric and morphology data. *J. Appl. Cryst.* **44**, 1272–1276 (2011).

Acknowledgments
Funding: This work was supported by the Deutsche Forschungsgemeinschaft (DFG, German Research Foundation), TRR 173-268565370 Spin + X: spin in its collective environment (projects B05 and B14). J.X. acknowledges Scientific Research Fund of Hunan Provincial Education Department of China (grant nos. 21B0548 and 19B159) and the National Natural Science Foundation of China (grant no. 11704114). J.V.B. and I.P.-Z. acknowledge funding by the Deutsche Forschungsgemeinschaft (DFG, German Research Foundation)–531278475.
Author contributions: L.L., M.Ae., and B.S. conceived the experiments. L.L. performed the STM and LEED experiments, and L.L. analyzed the data. L.L., T.E., and W.Y. carried out the ARPES and momentum microscopy measurements and analyzed the results. J.X. performed the DFT calculations, and L.L. and J.X. discussed and interpreted the data. Z.M.A.E.-F., M.As., I.P.-Z., and J.V.B. conducted and analyzed the EPWE simulations. L.L. and B.S. wrote the manuscript with input from all authors. **Competing interests:** The authors declare that they have no competing interests. **Data, code, and materials availability:** All data needed to evaluate and reproduce the conclusions in the paper are present in the paper and/or the Supplementary Materials. This study did not generate new materials.

Submitted 26 October 2025
Accepted 29 April 2026
Published 10 June 2026
10.1126/sciadv.aed3926

ScienceAdvances

Exploring the third dimension in quantum confinement of surface electrons

Lu Lyu, Tobias Eul, Wei Yao, Jin Xiao, Mostafa Ashoush, Zakaria M. Abd El-Fattah, Ignacio Piquero-Zulaica, Johannes V. Barth, Martin Aeschlimann, and Benjamin Stadtmüller

Sci. Adv. **12** (24), eaed3926. DOI: 10.1126/sciadv.aed3926